Monthly Notices
of the
ROYAL ASTRONOMICAL SOCIETY

Mon. Not. R. Astron. Soc. **403,** 1834–1848 (2010) doi:10.1111/j.1365-2966.2010.16288.x

Dynamical erosion of asteroid groups in the region of the Phocaea family

V. Carruba★

UNESP, Universidade Estadual Paulista, Grupo de Dinâmica Orbital e Planetologia, Guaratinguetá, SP 12516-410, Brazil

Accepted 2009 December 23. Received 2009 December 18; in original form 2009 November 10

ABSTRACT

In a previous paper, the current state of knowledge of the region containing the Phocaea dynamical family was revised. Here, the dynamical evolution and possible origin of the Phocaea dynamical family and asteroid groups in the region are investigated. First, I study the case of asteroids at high eccentricity ($e > 0.31$). I find that these objects are unstable because of encounters with Mars on time-scales of up to 270 Myr. The minimum time needed by members of the Phocaea classical family to reach the orbital locations of these objects, 370 Myr, can be used to set a lower limit on the age of the Phocaea family.

Next, attention is focused on the chaotic layer previously identified near the ν_6 secular resonance border. Using analytical and numerical tools, I find that the presence of the ν_6 secular resonance forces asteroids with $|g - g_6| < 2.55$ arcsec yr^{-1} to reach eccentricities high enough to allow them to experience deep, close encounters with Mars. Results of the analytical model of Yoshikawa and of my numerical simulations fully explain the low-inclination chaotic region found by Carruba.

Finally, I investigate the long-term stability of the minor families and clumps identified in the previous paper, with particular emphasis on a clump only identifiable in the domain of proper frequencies (n, g, $g - s$) around (6246) Komurotoru. I find that while the clumps identified in the space of proper elements quickly disperse when the Yarkovsky effect is considered, the family around (19536) is still observable for time-scales of more than 50 Myr. The (6246) clump, characterized by its interaction with the $\nu_5 + \nu_{16}$ and $2\nu_6 - \nu_{16}$ secular resonances, is robust on time-scales of 50 Myr. I confirm that this group may be the first clump ever detected in the frequency domain that can be associated with a real collisional event.

Key words: celestial mechanics – minor planets, asteroids.

1 INTRODUCTION

In Carruba (2009b), the current state of our knowledge regarding the Phocaea family region was revised. In that paper, among other things, families and clumps in the spaces of proper elements and proper frequencies were obtained and the current knowledge of asteroid taxonomy was revised, along with the albedo and absolute magnitude distribution of objects in the area. Furthermore, the dynamics of asteroids was studied using dynamical maps and chaos indicators. Several interesting results, like the identification of the first clump (around (6246) Komurotoru) that is only observable in the frequency domain, and an upper limit of 2.2 Gyr for the age of the family, were obtained in that paper.

Here I try to investigate the questions left unanswered by that work. Asteroids at high eccentricity, the orbits of which are characterized by very low values of Lyapunov time, may experience encounters with Mars that can quickly destabilize their orbits. In particular, I find that a population of asteroids at high e ($e > 0.31$) is unstable on time-scales of less than 270 Myr. The time needed by current members of the Phocaea classical family to reach the orbital location of these objects is of the order of 370 Myr, and can be taken as a lower limit on the otherwise not easily obtainable age of the Phocaea family.

Another question left unanswered by Carruba (2009b) concerns the cause and the stability of chaotic orbits near the ν_6 secular resonance border at the low-i boundary of the Phocaea family. Using analytical (Yoshikawa 1987) and numerical (Carruba et al. 2007) tools, in this work I study the effect of the proximity of the ν_6 secular resonance on asteroid eccentricity and find a simple analytical criterion to identify the asteroids most likely to present chaotic behaviour, as suggested in Carruba (2009b).

Finally, I investigate the long-term stability of the minor families and clumps identified in the previous paper, with particular emphasis on the clump only visible in the domain of proper frequencies (n, g, $g - s$) around (6246) Komurotoru. I find that while the clumps identified in the space of proper elements quickly disperse when the Yarkovsky effect is considered, the family around (19536)

★E-mail: vcarruba@feg.unesp.br

is still observable for time-scales of more than 50 Myr. The (6246) clump, characterized by its interaction with the $\nu_5 + \nu_{16}$ and $2\nu_6 - \nu_{16}$ secular resonances, is robust on time-scales of 50 Myr. I confirm that this group could be the first clump ever detected in the frequency domain alone that may be associated with a real collisional event.

The remainder of this paper is organized as follows. In Section 2 I review the preserving effect of the Lidov–Kozai resonance on highly inclined objects when planetary encounters are considered. In Sections 3 and 4 I investigate numerically the long-term stability of objects on highly eccentric orbits and the mechanisms that may replenish this asteroid population. In Section 5 I study the dynamics of chaotic orbits near the ν_6 resonance separatrix, while in Section 6 I investigate the long-term stability of minor families and clumps in the region. Finally, in Section 7 I present my conclusions.

2 THE LIDOV–KOZAI RESONANCE AND ITS CONSERVED QUANTITIES

It is well known that, under the effect of planetary perturbations, the argument of the pericentre ω of the orbit of a small body is forced to precess. In 1962, Lidov and Kozai pointed out that in the asteroid belt the precession of the argument of pericentre stops at large inclinations. The dynamics is then characterized by the libration of ω around $\pm 90^\circ$, locked into a resonance. This resonance is usually called the Lidov–Kozai resonance. Thomas & Morbidelli (1996) and Gronchi & Milani (1999) for the asteroid belt, and Carruba et al. (2002, 2004) for irregular satellites of Jovian planets, recently studied the secular behaviour of objects affected by this resonance. It can be shown (Thomas & Morbidelli 1996) that the Hamiltonian of a massless body perturbed by N planets on given orbits can be written as

$$H = H_0 + P = -\frac{1}{2L^2} - \sum_{j=1,N} m_j P_j(l, g, h, L, G, H), \qquad (1)$$

where m_j is the mass of the jth planet and P_J is a function of the Delaunay variables l, g, h, L, G and H ($l = M, g = \omega, h = \Omega, L = \sqrt{a}, G = \sqrt{a(1-e^2)}$ and $H = \sqrt{a(1-e^2)}\cos i$, where a denotes the semi-major axis, e the eccentricity, i the inclination (evaluated with respect to the invariable plane of the Solar system), Ω the longitude of the node, ω the argument of pericentre and M the mean anomaly of the massless body, respectively).

Since the Lidov–Kozai Hamiltonian after averaging over l and l_j does not depend on l and h, the Delaunay moments associated with these variables, L and H, are constants of the motion. As a consequence, the quantity $H = \sqrt{a(1-e^2)}\cos I$ is preserved ($\sqrt{a}$ is constant because of the conservation of L) in the averaged motion (Thomas & Morbidelli 1996; Gronchi & Milani 1999; Carruba et al. 2002). As discussed in Gronchi & Milani (1999), since the value of H is fixed from the initial conditions, both the averaged inclination and eccentricity have maximum allowed values:

$$I_{\max} = I(e = 0) = \arccos\frac{H}{\sqrt{a}}, \qquad (2)$$

$$e_{\max} = e(I = 0) = \sqrt{\frac{a - H^2}{a}}. \qquad (3)$$

When the eccentricity is large enough, the nodal distance at the ascending node,

$$d^+_{\rm nod} = \frac{a(1-e^2)}{1 + e\cos\omega} - a', \qquad (4)$$

and at the descending node,

$$d^-_{\rm nod} = \frac{a(1-e^2)}{1 - e\cos\omega} - a', \qquad (5)$$

between the ellipse of the asteroid orbit and the circular orbit (with radius a') of some perturbing planet can become zero. In this case a node-crossing is said to occur and a collision between the asteroid and the planet is possible. At $\omega = \pm 90^\circ$, $\cos\omega = 0$ and therefore the denominators in equations (4) and (5) become equal to 1. As a consequence, for values of ω for which the eccentricity is larger, the right-hand side of equations (4) and (5) reduces to its minimum value $a(1 - e^2) - a'$. The fact that for the maximal value of the eccentricity the nodal distance is not minimal is called the 'Lidov–Kozai protection mechanism'. For $\omega = 0^\circ$, equation (4) reduces to the first-order criterion $q = a'$, with q the asteroid pericentre distance $q = a(1 - e)$ (note that for $\omega = 0^\circ$ the value of the eccentricity is the minimum one).

In this section I consider what other information may be obtained by studying Lidov–Kozai conserved quantities in the region of the Phocaea dynamical family. For this purpose I start focusing my attention on the conserved values of the H integral.

Fig. 1(a) shows the current distribution of proper inclination and eccentricities for asteroids in the local background of the Phocaea family (black dots; see Carruba & Michtchenko 2009 for a definition of the Phocaea family local background), members of the Phocaea classical family (blue crosses) and members of the Phocaea

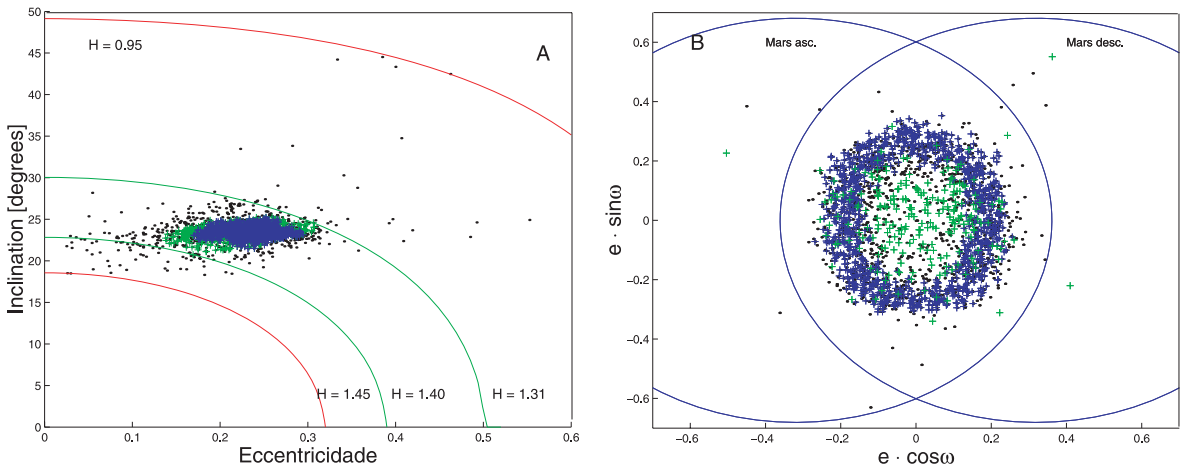

Figure 1. (a) (e, I) values of the H integrals for asteroids in the region of the Phocaea family. (b) Mars node-crossing lines for asteroids in the same region.

frequency family (green crosses). Superimposed are (e, I) values of the H integral in the range of H values for the Phocaea frequency family (green curves) and for the Phocaea local background (red curves).

Fig. 1(b) shows Mars node-crossing lines for asteroids with semi-major axis equal to that of the Phocaea classical family barycentre ($a = 2.3851$ au, Carruba 2009b), obtained with equations (4) and (5), assuming Mars is on a circular orbit of radius a'. As can be seen in the figure, all the members of the Phocaea classical family and the vast majority of the members of the Phocaea frequency family do not reach values of eccentricity large enough to experience a node-crossing with Mars. A few members of the Phocaea frequency family, however, reach eccentricities large enough to allow an interaction with Mars. I will investigate the long-term stability of these objects in the next section.

3 MARS-CROSSER ASTEROIDS IN THE REGION: NUMERICAL SIMULATIONS

As seen in the previous section and in Carruba (2009a), asteroids in the region of the Phocaea dynamical family at high eccentricities are characterized by interactions with Mars. In order to understand the long-term stability of asteroids in the region, I turn my attention to the results of numerical simulations. I start by performing short-term simulations on selected asteroids in the region.

3.1 Short-term numerical simulations

Since I am interested in studying Mars-interacting asteroids, I start by selecting objects with a non-zero possibility of interaction. In Carruba (2009a), I saw that a very simple criterion for identifying asteroids that possibly interact with Mars was to set $q = Q_{\rm Mars}$, with $q = a(1 - e)$ the pericentric distance of the asteroid and $Q_{\rm Mars} = a_{\rm Mars}(1 + e_{\rm Mars})$ the apocentric distance of Mars. In the previous section we saw that this is a simplistic criterion, and that a study of the nodal distance is more adequate to set limits on the Mars-interacting population. Nevertheless, the former criterion has the advantage of simplicity. Since I am interested in asteroids in the region of the Phocaea family, i.e. between the 7J:–2A resonance (approximately located at $a = 2.258$ au) and the 3J:–1A resonance (the left boundary of which is approximately located at $a \simeq 2.5$ au), I choose to work with asteroids with $e > 0.26$, which is the eccentricity of an asteroid with $q = Q_{\rm Mars}$ at the left boundary of the Phocaea dynamical family region, i.e. the 7J:–2A resonance. I remind the reader that all asteroids in this region are characterized by high inclinations, i.e. $\sin I > 0.3$. With these criteria, I identified 299 objects in the Phocaea local background.

Fig. 2(a) displays a proper (a, e) projection of these objects. Blue crosses are members of the Phocaea classical family and green crosses are members of the Phocaea frequency family. The green line displays the location for which $q = Q_{\rm Mars}$, the vertical red lines the locations of the main two- and three-body mean-motion resonances and the thick blue lines the location of the main secular resonances in the region.

As can be seen in the figure, the vast majority of the asteroids do not reach an eccentricity larger than 0.31. Only a few bodies, some possibly captured in the $2\nu_6 - \nu_{16}$ region, some captured by the 2M:–1A resonance and others that could possibly have interacted in the past with the 3J:–1A resonance, have eccentricity values larger than 0.31. To start investigating the orbital behaviour of these objects, I integrated the 299 asteroids with SWIFT-SKEEL, the symplectic integrator of Levison & Duncan (2000) that is able to model close encounters between a massive planet and a massless particle, over 20 Myr. Fig. 2(b) displays the values of maximal eccentricity attained by the integrated particles during the length of the simulation. Small blue dots display the initial orbital location in the proper (a, e) plane of the asteroids with $e_{\rm max} < 0.35$, medium-sized green dots show the orbital location of asteroids with $0.35 < e_{\rm max} < 0.40$, larger sized yellow dots display the orbits of asteroids with $0.40 < e_{\rm max} < 0.50$ and the largest red dots show the locations of asteroids with $e_{\rm max} > 0.5$ (during the length of the integration, three particles that reached values of $e_{\rm max} > 0.5$ were lost because of planetary close encounters). The other symbols are the same as in Fig. 2(a).

As can be seen in Fig. 2(b), the bodies with initial proper eccentricity > 0.31 are most of those characterized by $e_{\rm max} > 0.4$. To investigate the stability of orbits in the region further, I created a grid of test particles with initial osculating eccentricity between 0.20 and 0.40, for a range of semi-major axis between those of the 7J:–2A and 3J:–1A resonances, and with the values of inclination determined by the constancy of the H integral. In particular, I used a value of H equal to 1.3486, which is the median value of H for real asteroids in the region, once the high-e objects ($e > 0.4$) and high-I

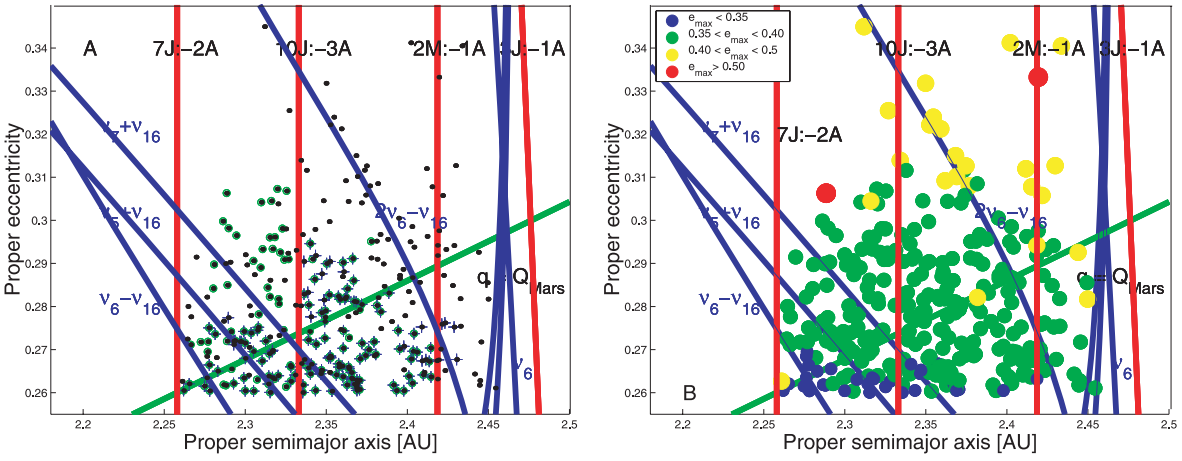

Figure 2. (a) An (a, e) projection of asteroids in the region of the Phocaea family, for $e > 0.26$. (b) The final status of the same asteroids at the end of the 20-Myr integration.

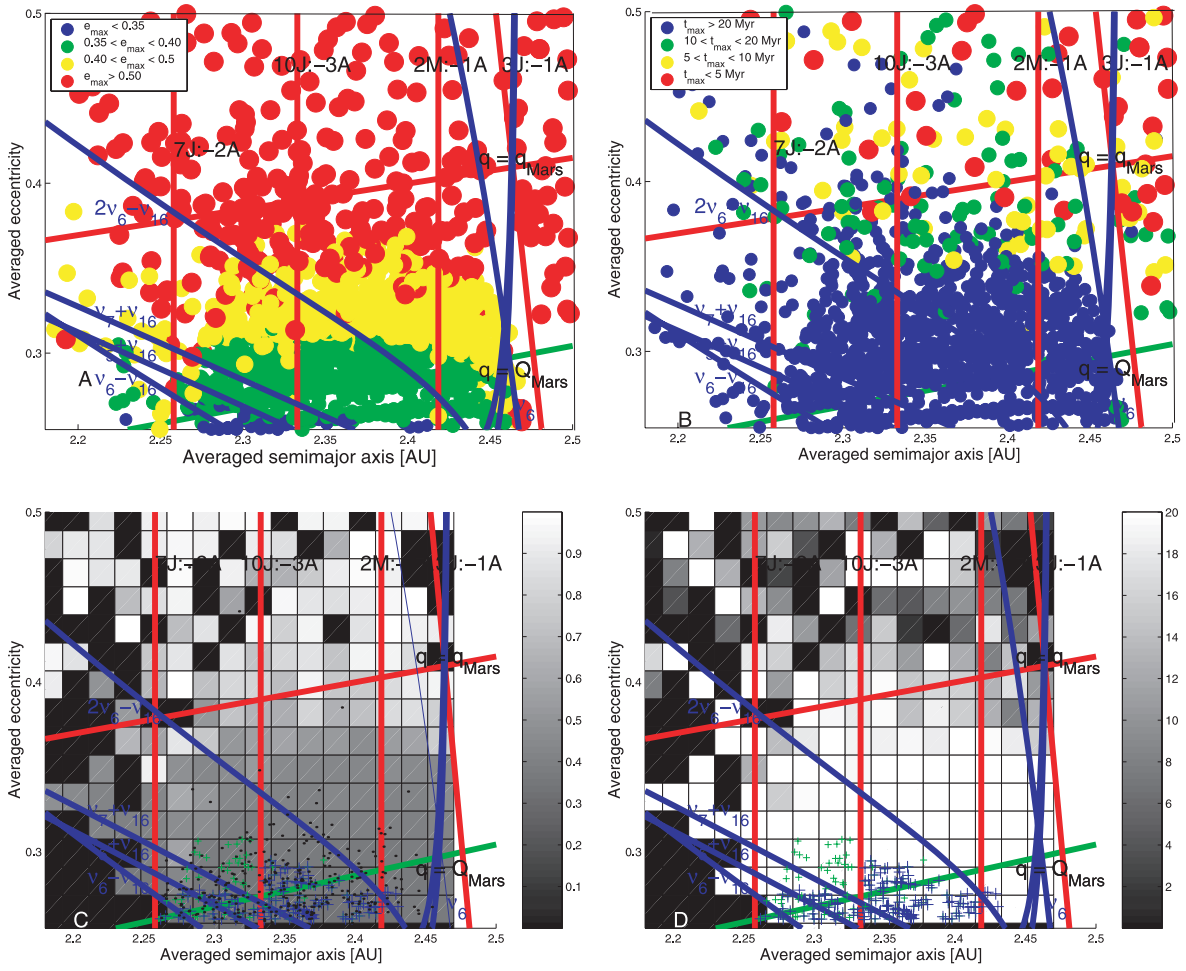

Figure 3. Projections in the space of averaged (a, e) of (a) maximum eccentricity values and (b) maximum survival time, for the simulated particles in the region. See text for a discussion of the colour code. Panels (c) and (d) display the position of real asteroids in the region, superimposed on density maps of maximum eccentricity and survival time.

objects ($\sin I > 0.45$) are excluded. The initial values of Ω, ω, and M were those of (77127) (2001 DJ93), an asteroid characterized by a value of $H = 1.3486$. There was a total of 2500 particles in this simulation, integrated over 20 Myr.

Fig. 3(a) shows a projection in the space of averaged (a, e) (the value of the mean of osculating elements during the integration length; I choose to work with mean elements rather than with proper elements because for many particles the survival time was too short to obtain a correct determination of proper elements) of the maximum osculating eccentricity achieved by the particle during the integration. The colour coding for the test particles and the other symbols is the same as in Fig. 2(b). Fig. 3(b) is similar, but shows the maximum survival times (see the figure legend for the description of the meaning of the particle colour codes).

As can be seen in the figures, particles with maximal value of eccentricity larger than 0.4 are confined to values of averaged eccentricity larger than 0.3. However, only particles with $e > 0.36$ were lost before the end of the integration (Fig. 3b). This is further confirmed by the density maps of $e_{\max}$ (Fig. 3c) and $t_{\max}$ (Fig. 3d). Following the approach of Carruba & Michtchenko (2009), in these figures I show the mean values of $e_{\max}$ and $t_{\max}$ on a grid covering the intervals (2.10–2.46) in a (I took 20 equally spaced intervals) and (0.225–0.5) in e (17 equally spaced intervals were used in this case). Superimposed on the density maps is the orbital location of asteroids in the background (black dots), in the Phocaea classical family (blue crosses) and in the Phocaea frequency family (green crosses), as obtained in Carruba (2009a).

During the length of the integration (20 Myr), particles in the region of real asteroids with $e > 0.31$ achieved larger values of maximal eccentricity, but they were not lost. To investigate further the long-term stability of asteroids in the region with $e > 0.31$, I performed simulations on longer time-scales for asteroids in this region. The set-up of the simulation and the results will be discussed in the next section.

3.2 Long-term stability of high-eccentricity objects

Fig. 2(a) displays an (a, e) projection of the 21 asteroids in the region of the Phocaea family. Of the objects with $e > 0.31$, (3343) Nezdel is the only one for which a spectral classification is available. Its S-type taxonomy is compatible with that of the Phocaea family. No information is available on the albedos of these objects.

As can be seen in Fig. 2(a), there are essentially six mechanisms that can increase an asteroid's eccentricity from the values observed in the region of the Phocaea family to $e > 0.31$: interaction with the 3J:–1A, 7J:–2A, 10J:–3A and 2M:–1A mean-motion resonances and interaction with the $\nu_5 - \nu_{16}$ and $2\nu_6 - \nu_{16}$ secular resonances. Of these mechanisms, the interaction of particles with the 3J:–1A

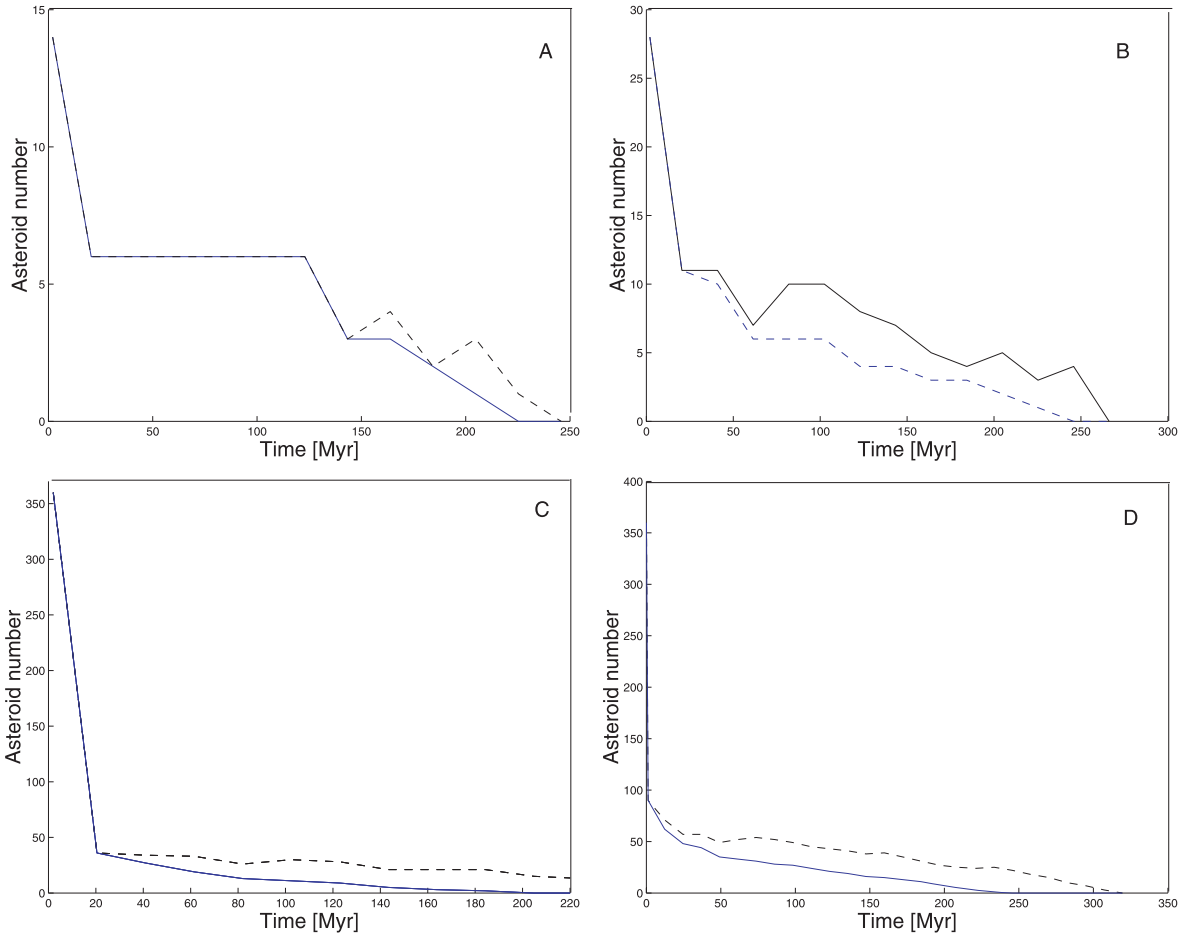

Figure 4. The number of objects (black line) and asteroids initially inside the high-e region defined in the text (blue dashed line), as a function of time. See text for a description of the different panels.

mean-motion resonance is a proven very effective mechanism in raising the eccentricity of test particles to Mars-crossing levels. In addition, the interplay of the Yarkovsky effect with the $\nu_5 + \nu_{16}$ and $2\nu_6 - \nu_{16}$ secular resonances and with the 2M:–1A mean-motion resonance may also increase the eccentricities of test particles to the level of the 21 observed objects with $e > 0.31$.

To investigate the long-term stability of these 21 asteroids further, I performed the following numerical experiments. First I integrated the 21 asteroids with SWIFT-SKEEL over 200 Myr under the gravitational influence of all planets from Venus to Neptune (Mercury was accounted for as a barycentric correction to the Sun's initial conditions). Following the approach of Nesvorný et al. (2008), I defined a region of interest which is between the 7J:–2A and and 3J:–1A mean-motion resonances and with $e > 0.31$, and checked how many objects remained in the area as a function of time during the numerical integration.

Fig. 4(a) shows this number as a function of time (black dashed line) and the number of objects initially in the area of interest that remained in the region as a function of time (blue line). I should emphasize that the parameter that gives information on the stability of objects is that related to the number of objects *initially* inside the area, i.e. the dashed line. The fact that other objects not originally in the area may be temporarily displaced inside the region of interest is, per se, not an indication of the stability of the initial asteroid population.

As can be seen in the figure, the number of high-e objects rapidly drops, tending to zero after 220 Myr if we consider the initial population and after 250 Myr if we consider the overall population of objects that passed through the region. As a second numerical experiment, I integrated the same particles with SWIFT_CE, an integrator developed in Carruba et al. (2007) that simultaneously models the effect of close encounters between a massive planet and a massless particle and the diurnal and seasonal versions of the Yarkovsky effect. I used typical values of Yarkovsky parameters for S-type asteroids (thermal conductivity $K = 0.001\,\mathrm{W\,m^{-1}\,K^{-1}}$, thermal capacity $C = 680\,\mathrm{J\,kg^{-1}\,K^{-1}}$, surface density $1500\,\mathrm{kg\,m^{-3}}$, density $2500\,\mathrm{kg\,m^{-3}}$, bond albedo 0.1 (Carruba et al. 2003), the asteroid radius computed using equation (1) in Carruba et al. (2003) and the average value of geometric albedo of Phocaea members, $p_V = (0.24 \pm 0.12)$ (Carruba 2009b)) and to one set of objects I gave an inclination of the spin axis of 90°, while to the second an obliquity of −90° was assigned. No re-orientations were considered, so that the drift caused by the Yarkovsky effect was the maximum possible.

Fig. 4(b) displays the number of objects in the area of interest, currently (black dashed line) and since the start of integration (blue line), during the length of the simulation. Similarly to the case without non-gravitational effects, the number of objects in the area drops quickly. Due to the interplay of the Yarkovsky effect with the $\nu_5 + \nu_{16}$ and $2\nu_6 - \nu_{16}$ secular resonances, which forced a few particles to stick to the resonances for longer, a few particles survived in the

high-eccentricity area for times up to 250 Myr. Eventually, all the initial population of resonant particles was lost after 270 Myr. I take this time as an upper limit on the stability of asteroids at high e.

One possible objection to these data is the low number of objects currently present at high e. To obtain a statistically more robust estimate of the stability time, I created a grid of 360 particles equally spaced in a by 0.005 au and in e by 0.004, in the range of a values 2.34–2.41 and of e values 0.26–0.352. The values of the other angles were obtained using the same procedure described in Section 3.1, and the test particles were integrated with both SWIFT_SKEEL and SWIFT_CE over 400 Myr. Again, I checked for the number of particles in the area around the $2\nu_6 - \nu_{16}$ resonance defined above. The results of my simulations are given in Figs 4(c) and (d). As can be seen in the figure, more than 90 per cent of the integrated test particles were lost in less than 20 Myr. For the integration with SWIFT_SKEEL, the last particle originally in the resonant area was lost after 200 Myr, while for the integration with SWIFT_CE the last particle was lost after 230 Myr. I believe that my integrations with a larger sample of test particles confirm that particles at high eccentricity are all lost by time-scales of at most of 270 Myr.

4 CREATING THE HIGH-ECCENTRICITY ASTEROID POPULATION

Now that I have investigated the stability of the high-eccentricity population, I want to understand on which time-scales the current population of 21 objects may be created starting from the orbital location of Phocaea family members. For this purpose, I selected 84 members of the classical Phocaea family with $a > 2.34$ au (these are particles that are able to interact with all of the major resonances that may increase their eccentricities, i.e. the 3J:–1A and 2M:–1A mean-motion resonances and the $\nu_5 + \nu_{16}$ and $2\nu_6 - \nu_{16}$ secular resonances; the other effective mechanism that can increase asteroid eccentricities, the ν_6 resonance, will be investigated in detail in Section 5) and created two clones for each of these particles. I integrated these clones with SWIFT_RMVSY.f, the symplectic code of Brož (1999), with the same set-up used for the SWIFT_CE integration over 400 Myr. I further divided the high-eccentricity area defined in Section 3.2 into two zones, Zone 1 with semi-major axis less than the value of the centre of the 2M:–1A resonance and Zone 2 between the 2M:–1A and 3J:–1A resonances, and I checked the number of objects that reached the resonant zones as a function of time.

Fig. 5 shows the number of objects that reached Zone 1, Zone 2 and the high-eccentricity region as a whole as a function of time. The first particle reached zone 1 only after 187 Myr of integration. It interacted with the 2M:–1A resonance, as did the only other particle that reached zone 1 during the integration. Four more particles reached the high-eccentricity zone 2. Of these, one interacted with the 3J:–1A resonance and was rapidly lost because of planetary close encounters, and three others interacted with the $\nu_5 - \nu_{16}$ secular resonance. On the whole, only six particles (7.14 per cent of the integrated bodies) achieved large values of eccentricity during the 370-Myr integration. While the sample that was integrated is somewhat limited to draw statistically significant conclusions from, I believe that the results obtained are sufficient to infer that, among the mechanisms that can produce a high-e population from the current Phocaea family members, the 3J:–1A, 2M:–1A and $\nu_5 - \nu_{16}$ resonances seems to be the most effective.

To test this hypothesis, I studied in detail the process of interaction of test particles evolving because of the Yarkovsky effect with each of the above-mentioned resonances. For each of the resonance

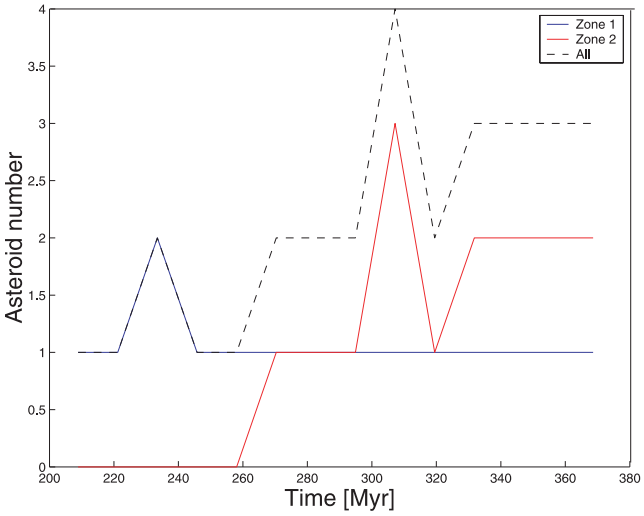

Figure 5. Number of asteroids that reached Zone 1 (blue line), Zone 2 (red line), and the high-eccentricity region as a whole (dashed black line) as a function of time. See text for the definition of Zones 1 and 2.

studies, I created test particles with spin inclinations of 90°, 60°, 30° and 15°, with positive values for particles with smaller semi-major axis than that of the resonance centre and negative ones for larger values of a. The other values of the Yarkovsky parameters are the same as used in the previous sections. I then let the test particles evolve and studied the changes in eccentricity caused by the interaction of the test particles with the resonances of interest. While the statistics of eccentricity changes provides far from a complete study of the resonance effect (which would involve a study of the resonance structure and the resonant angle at the time the particle was captured), I believe that this study may provide some first insights on the relative efficiency of the mechanisms studied in increasing the particle eccentricity.

The results of my simulations will be discussed in the next subsections.

4.1 3J:–1A resonance

The 3J:–1A mean-motion resonance is a well-known source of instability for asteroids in the inner main belt (see, among others, Morbidelli & Vokrouhlický 2003). It sets the lower limit in semi-major axis for the Phocaea dynamical family, and it is well known that a region of unstable chaotic orbits is found near the resonance separatrix (Guillens, Vieira Martins & Gomes 2002). Also, the non-linear dependence of the g frequency as a function of the semi-major axis in the proximity of the 3J:–1A resonance causes an increase in the density of secular resonances near the 3J:–1A resonance separatrix, as discussed in Carruba & Michtchenko (2009). Here I selected members of the Phocaea family with $a > 2.43$ au, which are the likeliest to interact with the 3J:–1A resonance. Fig. 6 displays their orbital location with respect to the 3J:–1A mean-motion resonance. The red line shows the location of the resonance separatrix, the magenta line the location of the chaotic layer near the resonance separatrix as defined in Morbidelli & Vokrouhlický (2003). Blue lines are associated with the main secular resonances in the region. Asteroids with Lyapunov times T_L larger than 50 000 yr are shown in red, asteroids with $20\,000 < T_L < 50\,000$ yr are shown in green and asteroids with $T_L < 20\,000$ are shown in black. One notices that the orbital behaviour of asteroids becomes more chaotic as they get closer to the layer of chaos near the resonance separatrix.

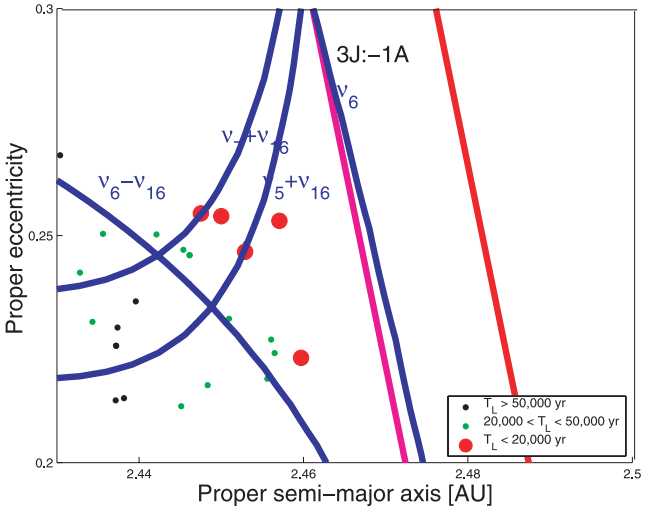

Figure 6. An (a, e) projection of Phocaea family members in the neighbourhood of the 3J:–1A resonance. See the text for an explanation of the other symbols.

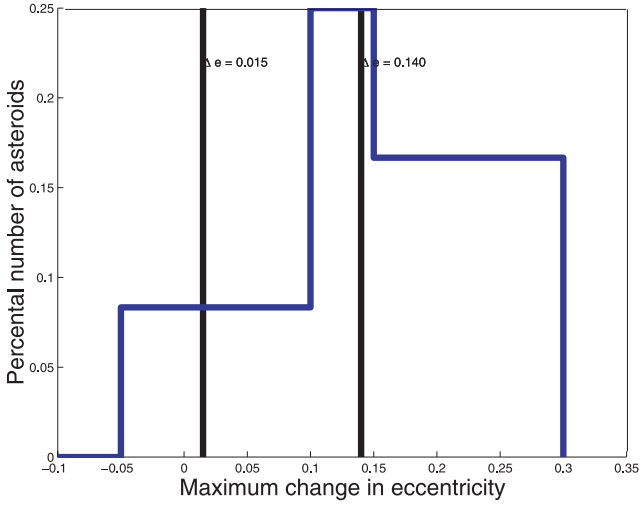

Figure 7. Histogram of maximal changes in eccentricity for particles in the simulation that interacted with the J7:–2A mean-motion resonance.

To study the interaction of family members with the 3J:–1A resonance, I selected 17 objects with $a > 2.43$ au and gave them the four positive values of orbital spins described in Section 4. As expected, none of the integrated particles survived the extent of the simulation. Before reaching the 3J:–1A mean-motion resonance, the test particles interacted with the ν_6 secular resonance, the proximity of which significantly increased the values of their eccentricity with a mechanism that will be described in detail in Section 5. This mechanism alone was sufficient to push the eccentricity of at least 56.4 per cent of the integrated test particles to Mars-crossing values, causing their loss. The remaining 44.6 per cent of particles, which survived the passage through the ν_6 secular resonance, did not survive the interaction with the 3J:–1A mean-motion resonance. Most of these particles had their eccentricity raised to Mars-crossing and Earth-crossing values with a mechanism well studied analytically (Ferraz-Mello et al. 1996) and numerically (Gladman et al. 1997), and were rapidly lost. Overall, I observed 35 particles that were pushed to the Zone 1 defined in Section 4 and then lost with timescales compatible with the results of Section 3.2. Based on these results, I believe that interaction with the J3:–1A mean-motion resonance (and the near ν_6 secular resonance) may be a valid mechanism to produce the currently observed $e > 0.31$ population.

4.2 7J:–2A resonance

The 7J:–2A mean-motion resonance sets the leftward limit in proper semi-major axis for the Phocaea dynamical family (only one family member, (57308) 2001 QL201, has a semi-major axis value less than the J7:–2A resonance centre). For that reason, I selected six asteroids within 0.01 au of the J7:–2A resonance centre, and I assigned to them only the four negative values of spin discussed in Section 4, so that their semi-major axis evolution will cause them to interact with the J7:–2A resonance.

Fig. 7 displays the changes in eccentricities caused by the passage through the J7:–2A resonance for my test particles. Vertical lines display the minimum and maximum change in eccentricity needed by a member of the Phocaea classical family to reach the $e > 0.31$ region. As can be seen in the histogram, there was only one case where there was a decrease in eccentricity. Most of the other particles experienced positive changes with Δe up to 0.25, more than enough to reach the 0.31 value from typical Phocaea family values of eccentricity. Most of the particles, due to their spin-axis orientation, evolved toward smaller values of semi-major axis and exited from the Phocaea local background. While it is possible that some of the particles with eccentricity increased beyond 0.31 may invert their spin-axis orientation and evolve towards the Phocaea local background, I also observed a few cases in which close encounters with Mars pushed back asteroids that passed through 7J:–2A in the Phocaea local background region. Based on these considerations, I believe that interaction with the 7J:–2A mean-motion resonance may be considered an effective mechanism for producing the currently observed high-eccentricity population.

4.3 2M:–1A resonance

As observed in Section 4, the 2M:–1A mean-motion resonance may be an effective mechanism for increasing the eccentricity of members of the Phocaea family to values larger than 0.31. To test the efficiency of this resonance in increasing particle eccentricities, I integrated 60 particles with a smaller than the resonance centre value (15 real asteroids with the four values of positive spin inclination described in Section 4) and 52 particles with a larger than the resonance centre value (13 particles, with four values of negative spin inclination).

Fig. 8 displays a histogram of maximal eccentricity changes for particles that interacted with the 2M:–1A resonance during the length of the 200-Myr numerical simulation with SWIFT_RMVSY.f. As can be seen in the figure, most of the particles experienced small variations in eccentricity when passing through the 2M:–1A resonance ($\Delta \simeq 0.001$), but about 15 per cent of the integrated test particles achieved values of $\Delta e > 0.05$. The largest negative values of Δe were found in test particles with positive spin values, but larger positive values of Δe were observed for this simulation as well. This seems to confirm that evolution in the 2M:–1A mean-motion resonance may be a viable mechanism to produce high-eccentricity objects.

4.4 $\nu_5 + \nu_{16}$ secular resonance

Another mechanism to increase particle eccentricity, the efficiency of which needs to be tested, is that of the interaction of the

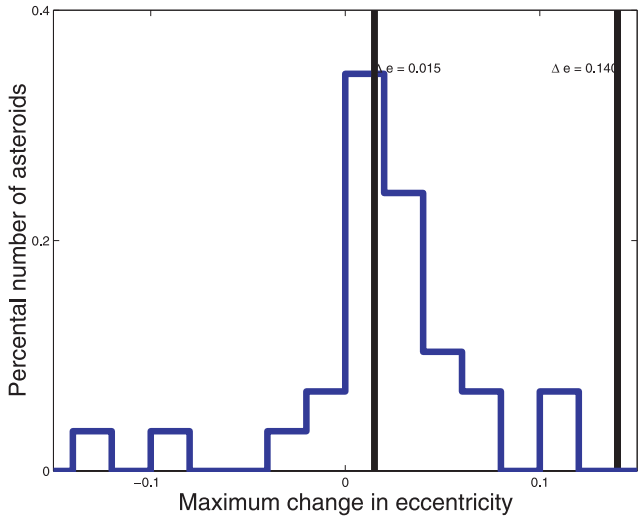

Figure 8. Histogram of maximal changes in eccentricity for particles in the simulation that interacted with the 2M:–1A mean-motion resonance.

$\nu_5 + \nu_{16}$ secular resonance with the Yarkovsky and YORP effects.[1] To test this mechanism, I selected 11 particles within ± 0.5 arcsec yr^{-1} of the resonance centre, for values of the semi-major axis larger than that of the 2M:–1A mean motion resonance and smaller than the 10J:–3A mean-motion resonance. Asteroids in the $\nu_5 + \nu_{16}$ secular resonance in between these two resonances have values of eccentricity too small to be a significant source of the high-eccentricity population (see Figs 2a and b). I assigned to these asteroids the eight values of spin obliquities discussed in Section 4 and integrated them over 200 Myr with SWIFT-RMVSY.

I analysed the resonant argument of the $\nu_5 + \nu_{16}$ secular resonance for the 88 particles that I integrated and found that 51 of them (58.0 per cent of the total) remained in librating states during the length of the integration, 32 (36.4 per cent) passed through the resonance or alternated phases of libration and circulation, and five of them (5.5 per cent) were not in resonant states. The orbital behaviour of librating particles showed characteristic oscillations in eccentricity of the order of the resonant argument librating period ($\simeq$5 Myr), which did not alter the particle eccentricity significantly during an oscillation period. Changes on longer time-scales were observed for a few particles, but were of minor importance (of the order of 0.02 at most, over 200 Myr) and, unfortunately, directed in the 'wrong' direction to explain the currently observed population of $e > 0.31$ asteroids. Particles with positive changes in e either evolved toward the J3:–1A resonance and had semi-major axis larger than that of the M2:–1A resonance (i.e. they could at best be objects created in Zone 2, as defined in Section 4) or evolved beyond the 10J:–3A resonance, outside the boundaries of Zone 1. Neither of these test cases could therefore have created the observed population of high-e objects.

For particles that crossed the $\nu_5 + \nu_{16}$ secular resonance, or its Uranian twin the $\nu_7 + \nu_{16}$ resonance, the highest change in eccentricity observed was 0.015, which is just barely enough to push the highest eccentricity members of the classical Phocaea family into the $e > 0.31$ region.

In view of these considerations, I believe that interaction with the $\nu_5 + \nu_{16}$ secular resonance may have had played at best an auxiliary role in the creation of the currently observed high-eccentricity population.

4.5 $2\nu_6 - \nu_{16}$ secular resonance

As was seen in Figs 2(a) and (b), most of the $e > 0.31$ population was found in proximity to the $2\nu_6 - \nu_{16}$ secular resonance. Can the interplay of this resonance with the Yarkovsky and YORP effects explain the current presence of some high-eccentricity objects? To test this hypothesis I selected 15 members of the Phocaea classical family, the $2g - s$ values of which were within ± 1.5 arcsec yr^{-1} from the resonance value. Five of these objects had semi-major axis larger than the resonance semi-major axis and were given the four negative values of spin obliquities discussed in Section 4, while the other 10 had smaller semi-major axis than the resonance centre and were given the four positive values of spin obliquities.

I integrated these objects over 200 Myr with SWIFT-RMVSY, and checked for each particle the resonant argument of the $2\nu_6 - \nu_{16}$ secular resonance. At the end of the integration only three particles (5 per cent of the total) were still inside the resonance. Passage through the resonance or the secular change caused by the resonant evolution in e was at most of order 0.010, insufficient to push even the more eccentric members of the Phocaea classical family inside the high-eccentricity region $e > 0.31$. Based on these considerations, I conclude that the $2\nu_6 - \nu_{16}$ secular resonance played at best a minor role in the creation of the currently observed high-e population. The alignment of asteroids at the centre of the $2\nu_6 - \nu_{16}$ secular resonance observed in Fig. 2 may therefore be just an artefact created by the procedure used to obtain synthetic proper elements, which causes asteroids in or near a secular resonance to appear at the resonance centre due to averaging over more than a libration period in the resonance (Knežević & Milani 2003).

5 CHAOTIC DYNAMICS NEAR THE ν_6 RESONANCE SEPARATRIX

One of the questions left unanswered by Carruba (2009b) was the cause of the chaotic dynamics near the ν_6 resonance separatrix. In this section I will investigate this problem with analytical and numerical tools.

5.1 Analytical model of the ν_6 secular resonance

Since the late 1980s, it has been known that asteroids in the proximity of the ν_6 secular resonance have their eccentricity raised to planetary-crossing values and are so destabilized on short time-scales (see, among others, Yoshikawa 1987). To estimate the effect of the proximity of the ν_6 secular resonance more quantitatively here, I briefly revise the non-linear model of Yoshikawa (1987) for the ν_6 resonance. In his model Yoshikawa kept terms up to third degree in eccentricity and inclination for the secular part of the disturbing function, and, under the hypothesis of proximity to the ν_6 resonance, assuming $l_6 = \varpi - \varpi_6^*$ moves much more slowly than $l_5 = \varpi - \varpi_5^*$, where $\varpi_i^* = \nu_i \cdot t + \beta_i$, and ν_i and β_i are known constants (Bretagnon 1974), obtained the following expression for the Hamiltonian of the problem:

$$F_{\nu_6} = \frac{1}{2}(b - \nu_6)e^2 + \frac{1}{4}ce^4 - d_6 e \cos(\varpi - \varpi_6^*), \quad (6)$$

[1] Due to the small difference in arcsec yr^{-1} between $g_5 = 4.257$ arcsec yr^{-1} and $g_7 = 3.093$ arcsec yr^{-1}, the $\nu_5 + \nu_{16}$ secular resonance is close in proper element space to the $\nu_7 + \nu_{16}$ resonance. Since resonances involving the g_5 frequency have a stronger effect on asteroid proper elements (Milani & Knežević 1994; Carruba & Michtchenko 2007, 2009), here I will focus my attention on the resonance involving the Jovian frequency.

where $\nu_6 = 26.217$ arcsec yr^{-1} is the value of the precession frequency of the pericentre of Saturn and b, c and d_6 are coefficients with values given by

$$b = \frac{1}{na^2}\sum_{j=1}^{8} Gm_j[2A_j + 2D_j \sin^2(i) + C_j \sin(2i)\tan(i/2)], \tag{7}$$

$$c = \frac{1}{na^2}\sum_{j=1}^{8} Gm_j(4B_j - A_j), \tag{8}$$

$$d_i = -\frac{1}{na^2}\sum_{j=1}^{8} Gm_j E_j M_{ji}, \tag{9}$$

where m_j is the mass of the jth planet, M_{ji} are constants given in Bretagnon (1974) and expressions for the A_j, B_j, C_j, D_j, E_j coefficients are given by

$$A_j = \frac{1}{8a'}\alpha b^{(1)}_{3/2}, \tag{10}$$

$$B_j = \frac{1}{16a'}\left[\frac{1}{2}\alpha^3\frac{d^3 b^{(0)}_{1/2}}{d\alpha^3} + \frac{1}{8}\alpha^4\frac{d^4 b^{(0)}_{1/2}}{d\alpha^4}\right], \tag{11}$$

$$C_j = -\frac{1}{8a'}\alpha b^{(1)}_{3/2}, \tag{12}$$

$$D_j = \frac{1}{16a'}\left[-\alpha b^{(1)}_{(3/2)} - 2\alpha^2\frac{db^{(1)}_{3/2}}{d\alpha} - \frac{1}{2}\alpha^3\frac{d^2 b^{(1)}_{3/2}}{d\alpha^2}\right], \tag{13}$$

$$E_j = -\frac{1}{4a'}\alpha b^{(2)}_{3/2}, \tag{14}$$

where

$$\alpha = a/a_j, \quad a' = a_j \quad (a_j > a), \tag{15}$$

$$\alpha = a_j/a, \quad a' = a \quad (a_j < a). \tag{16}$$

The Laplace coefficients $b^{(m)}_s(\alpha)$ (with s a semi-integer number) are defined by

$$b^{(m)}_s(\alpha) = \frac{2}{\pi}\int_0^{\pi}\frac{\cos(m\theta)\,\mathrm{d}\theta}{(1 - 2\alpha\cos\theta + \alpha^2)}. \tag{17}$$

Useful expansions in series of α for the Laplace coefficients and relations between the Laplace coefficients and its derivatives are given in Murray & Dermott (1999), equations (6.68)–(6.72). To check if my numerical computation of the b, c and d_i coefficients agrees with that of Yoshikawa (1987), here I re-obtained b as a function of a and chosen values of i and c and d_5 and d_6 as functions of a (Figs 9a and b). The results are in excellent agreement with figs 3 and 4 of Yoshikawa (1987).

In this paper I am interested in investigating the dynamics of objects near the ν_6 resonance separatrix. Following Yoshikawa (1987), I introduce the k_6 parameter:

$$k_6 = b - \nu 6. \tag{18}$$

In the Phocaea family range of inclination values, only negative values of k_6 are observed. A limiting value of $k_6 = -2.55$ arcsec yr^{-1} can be introduced to discriminate between two classes of orbital behaviour, based on the following considerations. Using equation (6) I can compute values of the ν_6 Hamiltonian in the $(\varpi - \varpi_6{}^*, e)$ plane, for $\varpi - \varpi_6{}^*$ in the range 0°–360° and e from 0–0.6 (the accuracy of the Yoshikawa model drops at higher eccentricities). Fig. 10 displays the resulting contour plots for (a) a body with $k_6 = -0.29$ arcsec yr^{-1}, (b) a body with $k_6 = -2.55$ arcsec yr^{-1} and (c) an asteroid with $k_6 = -5.00$ arcsec yr^{-1}. The black line displays the level $F_{\nu_6} = 0$, red lines negative values of F_{ν_6} and blue lines positive values. The horizontal line shows the $e = 0.31$ level, which corresponds to eccentricity values that I found to be unstable on time-scales of up to 270 Myr in Section 3.2. Generally speaking, for any value of k_6 I observe an island of libration at negative energies centred at $\varpi - \varpi_6{}^* = 180°$ and another island of libration at positive energies centred at $\varpi - \varpi_6{}^* = 0°$.

Depending on the value of k_6, two different orbital behaviours for the libration island at $\varpi - \varpi_6{}^* = 180°$ are observed. For $k_6 > -2.55$ arcsec yr^{-1}, orbits in this libration island are forced to reach values of eccentricity higher than 0.31 for *any* value of initial eccentricity, because of the presence of the second libration island at $\varpi - \varpi_6{}^* = 0°$ (Figs 10a and b).

For $k_6 < -2.55$ arcsec yr^{-1} (Fig. 10c), however, all orbits in the libration island at $\varpi - \varpi_6{}^* = 0°$ and some of the orbits in the libration island at $\varpi - \varpi_6{}^* = 180°$ reach values of maximal eccentricity well below 0.31, and are therefore protected from the effect of planetary close encounters.

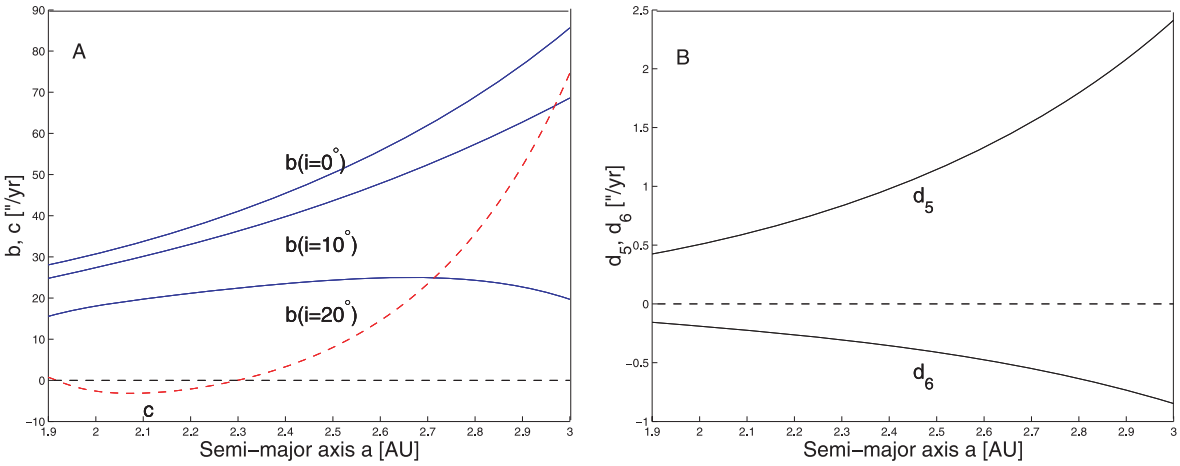

Figure 9. (a) Dependence of the b and c parameters of Yoshikawa (1987) on the semi-major axis and chosen values of inclination. (b) Dependence of d_5 and d_6 on the semi-major axis.

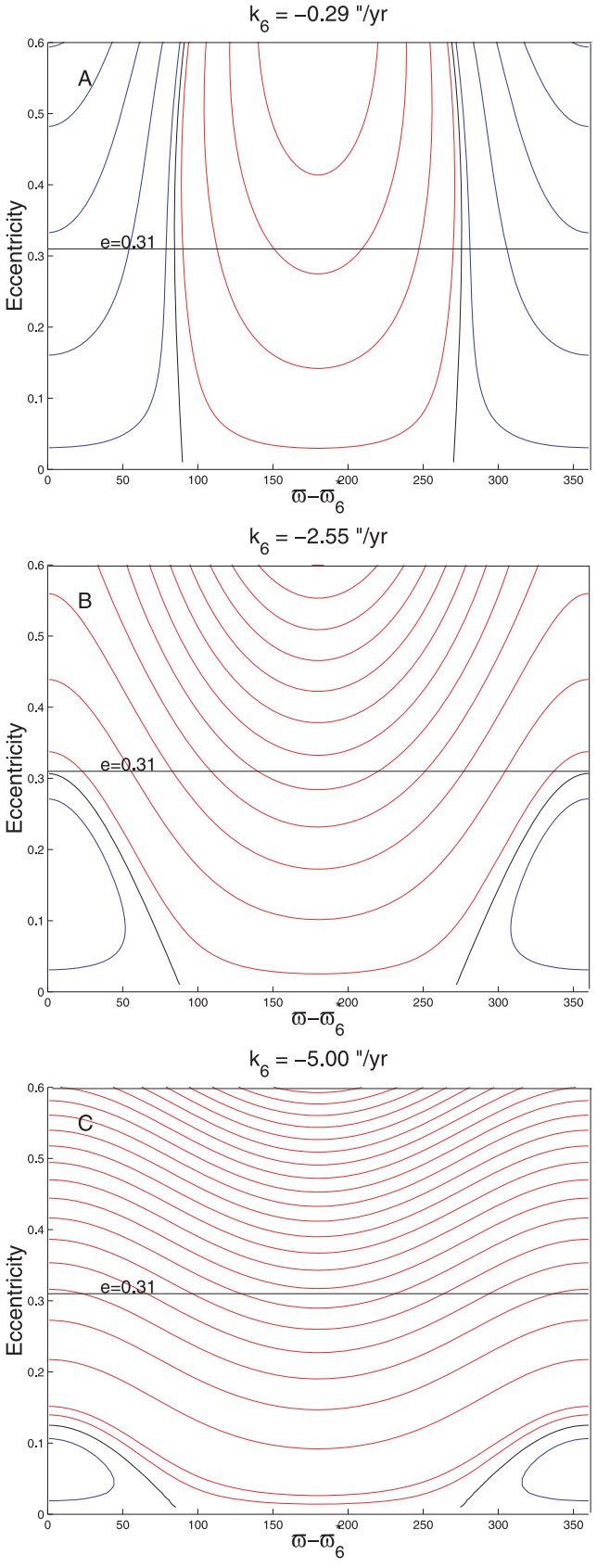

Figure 10. Contour plots of Hamiltonian values for asteroids with (a) $k_6 = -0.29$ arcsec yr^{-1}, (b) $k_6 = -2.55$ arcsec yr^{-1} and (c) $k_6 = -5.00$ arcsec yr^{-1}. The horizontal lines display the limiting value of $e = 0.31$.

Can the effect of the proximity of the ν_6 secular resonance be responsible for the lower density of objects with $-2.55 < k_6 < 2.55$ arcsec yr^{-1}? To investigate this possibility further I turn my attention to the results of numerical simulations for real and fictitious objects in the region.

5.2 Numerical simulations

In Carruba (2009b), a zone of small Lyapunov times near the separatrix of the ν_6 secular resonance was identified. The causes of the chaotic behaviour were, however, left as an unanswered question. In the previous section we saw that near the separatrix of the ν_6 secular resonance and for values of k_6 in the range $-2.55 < k_6 < 2.55$ arcsec yr^{-1} orbits are forced to reach values of eccentricities larger than 0.31, a value for which deep close encounters with Mars are possible. To confirm further that the chaotic behaviour of small-inclination asteroids is indeed caused by the ν_6 secular resonance, I computed values of k_6 for the test particles that I used for my estimates of Lyapunov times in the (a, sin (i)) plane in Carruba (2009b). Fig. 11(a) displays an enlarged view of the low-inclination region of small Lyapunov times found in Carruba (2009b), while Fig. 11(b) shows the orbital location of $-2.55 < k_6 < 2.55$ arcsec yr^{-1} asteroids in the space of averaged (a, sin (i)) (red full dots). The agreement between the two figures is stunning: the core of chaotic behaviour is clearly associated with the $-2.55 < k_6 < 2.55$ arcsec yr^{-1} region, with a few extra particles at slightly larger inclination that are associated with particles that do not reach $e = 0.31$ but are still able to experience shallow Martian close encounters, as observed during the simulation. I believe that this result fully explains the causes of the chaotic behaviour found in Carruba (2009b).

What about the long-term stability of the current low-inclination objects in the Phocaea family local background? As seen in Fig. 11(a) and in fig. 12(b) of Carruba (2009b), real objects are currently in regions of regular behaviour, characterized by $k_6 < -2.55$ arcsec yr^{-1}, so we would expect them to be relatively stable. To answer this question here I identified real asteroids in that region and numerically studied their long-term stability. I chose asteroids in the Phocaea local background as defined in Carruba & Michtchenko (2009), with a value of sin (i) smaller than the minimal value observed in the Phocaea frequency family (sin (i) = 0.3556) and with a range of semi-major axis between the 7J:–2A and 3J:–1A mean-motion resonances. Objects with inclination smaller than that of the centre of the ν_6 secular resonance were also excluded from the sample. There were 44 objects that satisfied this requirement, and I integrated them with SWIFT_CE and the same Yarkovsky parameters used in previous runs and a similar planetary set-up, over 200 Myr. I then checked how many particles remained in the low-inclination region that I defined above as a function of time.

Apart from two test particles that interacted with the 3J:–1A resonance and were lost, all the other particles remained in the low-inclination region during the length of the integration, thus confirming the stability of the current low-i population. While all of the test particles were considerably far away from the $-2.55 < k_6 < 2.55$ arcsec yr^{-1} region, the three asteroids at lowest inclination, (87112) (2000 LB25), (111923) (2002 GW17) and (142401) (2002 SH23), displayed an orbital behaviour compatible with that observed in Fig. 10(b) (the actual orbital evolution in the ($\varpi - \varpi_6$, e) plane did not of course completely follow the Hamiltonian F_{ν_6} of equation (6), because of the fact that further away from the ν_6 separatrix the approximation that $l_5 = \varpi - \varpi_5^*$ no longer holds),

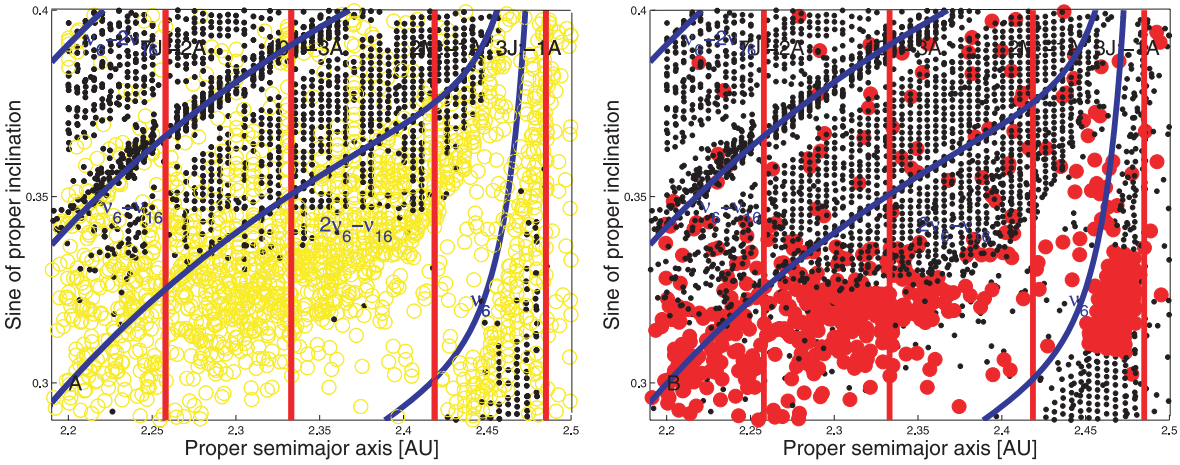

Figure 11. (a) Lyapunov times projected in the space of averaged (a, sin (i)) elements. Yellow circles display Lyapunov times smaller than 20 000 yr, while black dots are associated with times larger than 20 000 yr. (b) k_6 values in the same range of averaged (a, sin (i)) elements. Red full dots display values of k_6 in the range $-2.55 < k_6 < 2.55$ arcsec yr^{-1}.

and occasionally reached large values of osculating eccentricity (up to 0.35 for (111923) (2002 GW17)). While none of the three low-i asteroids was lost during the simulation, the fact that these three objects experienced episodes of high osculating eccentricity may explain why a region of low number density of asteroids at low i outside the $-2.55 < k_6 < 2.55$ arcsec yr^{-1} region was found in Carruba (2009b) (Figs 3c and d).

6 LONG-TERM STABILITY OF MINOR FAMILIES AND CLUMPS IN THE REGION

In Carruba (2009a), several small dynamical groups were identified in the region of the Phocaea dynamical family. Many of these groups had a limited number of members, sometimes just large enough for the group to be considered a clump. A question left unanswered by the previous work concerned the statistical significance of these groups. Were these clusters created by real collisions or were they just random association of bodies that happened to be in nearby orbits for a limited period of time? In order to estimate the statistical significance and the time-scales over which these clusters are still bound, I devised the following numerical experiment: I created two sets of clones of members of the clusters and integrated them with SWIFT-RMVSY.f, the symplectic integrator of Brož (1999) that simulates the diurnal and seasonal version of the Yarkovsky effect. Using typical values of the Yarkovsky parameters (Carruba et al. 2003) I gave to one set of objects an inclination of the spin axis of 90°, while to the second was assigned an obliquity of −90°. No re-orientations were considered, so that the drift caused by the Yarkovsky effect was the maximum possible.

I integrated the clones of members of the classical and frequency clusters over 200 Myr in the future and 200 Myr in the past[2] and obtained synthetic proper elements according to the definition of Knežević & Milani (2000) for the clones every 2.4576 Myr. I then re-obtained families and clumps for the set of synthetic proper elements of the clones at each time-step, using the barycentre of the clusters (Carruba 2009a, equation 7) as the first body for the family. As soon as the cluster (obtained for a value of velocity cut-off of 160 m s^{-1} and of frequency cut-off of 0.625 arcsec yr^{-1}, as in Carruba 2009a) failed to reach the minimum number of objects required to be considered a clump, the cluster was considered dispersed and a minimum limit for the dispersion time was found.

I will start by discussing the results for the classical families and clumps in the next subsection.

6.1 Classical groups

In Carruba (2009a), two minor clumps (one around (17628) (1996 FB5), the other one around (26142) (1994 PL1), both with 10 members) and a family (around (19536) (1999 JM4), with 27 members; this family merges with the asteroid associated with the Gil–Hutton clump (2860) Pasacentennium at a cut-off of 164 m s^{-1}) were identified in the space of proper elements. Here I start my analysis investigating the two clumps.

Fig. 12 displays the number of members of (a) the (17628) clump and (b) the (26142) clump as a function of time. As can be seen in the figure, except for isolated spikes for which the number of members occasionally rises above the clump level ($n = 9$ at a $v_{\rm cut-off} = 160$ m s^{-1}, horizontal line in the figure), both clumps are not recognizable as such for most of the integration length. Based on this consideration, I believe the two clumps may just be considered as statistical flukes. This is also confirmed by the fact that neither clump is recognizable in the space of proper frequencies (n, g, $g - s$) (Carruba 2009a).

Things are different for the case of the family around (19536). This family is recognizable in the space of proper frequencies (see next subsection for the discussion of this case) and it appears to be statistically robust: Fig. 13(a) displays the number of family members as a function of time, detected at a cut-off of 160 m s^{-1}. The horizontal green line displays the minimum number of members for the group to be identifiable as a family at this cut-off ($n = 22$). Notice that the family is still detectable for time-scales up to 190 Myr. Many of the family members are characterized by their interaction with the $\nu_6 - 2\nu_{16}$ secular resonance. At the beginning of the simulation, 26 particles were in the $\nu_6 - 2\,\nu_{16}$ librating state.

[2] Concerning the integration in the past, I should caution the reader that integrations with the Yarkovsky effect are not conservative, and therefore technically speaking not time-reversible. Backward integrations are however interesting from a statistical point of view, and while they are not accurate for a single asteroid, they still provide useful information for a statistically significant sample of objects.

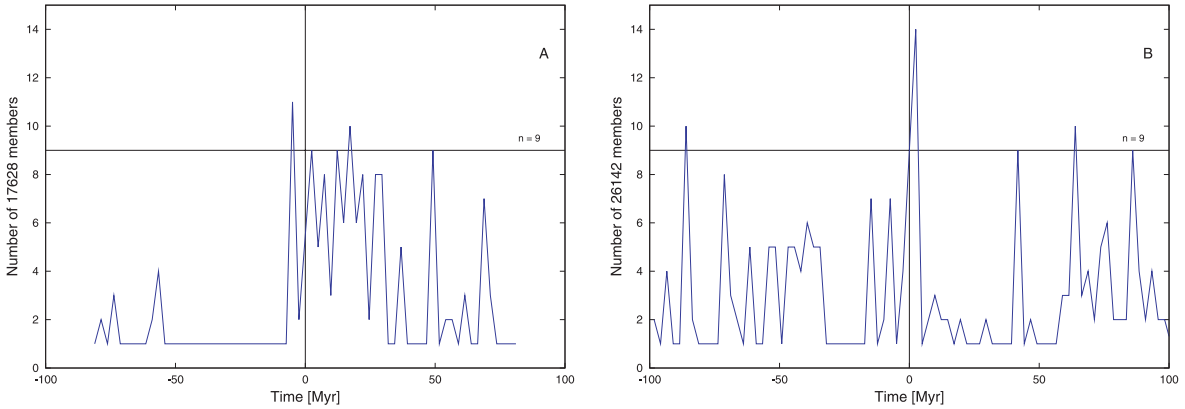

Figure 12. The number of members of (a) the (17628) clump and (b) the (26142) clump as a function of time.

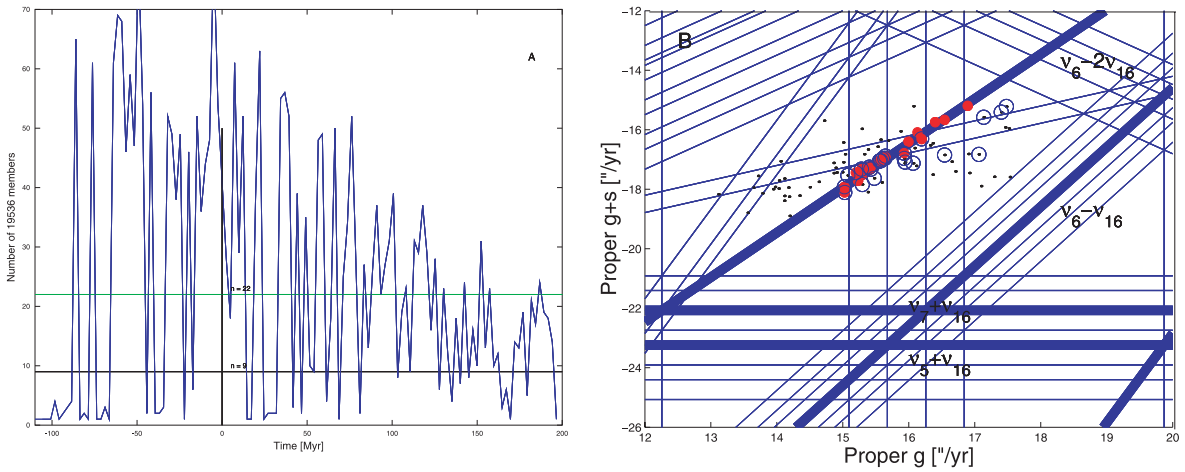

Figure 13. (a) The number of members of the 19536 classical family detected at a cut-off of 160 m s^{-1} as a function of time. (b) A (g, $g - s$) projection of the family clones at $t = 190$ Myr. The blue circles identify the clump members, the red full dots the asteroids in a librating $\nu_6 - 2\nu_{16}$ resonant state.

Fig. 13(b) displays a (g, $g + s$) projection of the family clone at $t =$ 190 Myr, the last time for which the family was still identifiable. Red full dots show asteroids in the $\nu_6 - 2\nu_{16}$ resonance, blue circles the members of the family and black dots the orbital location of all particles. Considering that the family was observable for more than 190 Myr into the future, and for more than 90 Myr in the past, I conclude that the group can be considered a good candidate for a collisional family.

6.2 Frequency groups

In the (n, g, $g - s$) frequency domain I identified two minor clumps in the region of the Phocaea family (Carruba 2009a): one around (19536) (1999 JM4) with 14 members at a cut-off of 0.625 arcsec yr^{-1} and another around (6246) Komurotoru, with nine members at the same cut-off. Of the two, the most interesting one was the clump around (6246), since this one was identifiable in the frequency domain only. Here I want to investigate how stable in time the clumps that I identified in Paper I (Carruba 2009b) are. I start my analysis with the clump around (6246) Komurotoru.

This clump is characterized by its interaction with two secular resonances: the $\nu_5 + \nu_{16}$ and the $2\nu_6 - \nu_{16}$ resonances. Of the 50 particles that I integrated (there were 25 members of the clump at the maximum cut-off of 0.745 arcsec yr^{-1}), six objects were in a $\nu_5 + \nu_{16}$ librating state during the whole simulation and four in a $2\nu_6 - \nu_{16}$ resonant state. 15 other particles had phases of libration in one of the two resonances during the integration. Fig. 14 displays the resonant angles of two particles trapped in the the $\nu_5 + \nu_{16}$ and $2\nu_6 - \nu_{16}$ resonances respectively. The thick red line displays the resonant argument passed through a digital filter so as to eliminate all frequencies with periods less than 1 Myr (see Carruba et al. 2005 for a discussion of the digital filtering procedure).

Fig. 15 displays the number of members of the 6246 frequency clumps in the Phocaea family region as a function of time. Panel (a) displays the data for a frequency cut-off of 0.625 arcsec yr^{-1}, while panel (b) shows the same for a cut-off of 0.745 arcsec yr^{-1}. While the numbers of members are obviously higher for the clumps found with the higher cut-off, the qualitative behaviour is roughly the same: after $\simeq$50 Myr the clump members disperse and they are no longer recognizable as a dynamical group, while for the integration backward in time the clump was identifiable up to -200 Myr. The fact that the clump is still identifiable before 200 Myr and after 50 Myr seems to indicate that it may be a robust dynamical group, and not just a statistical fluke.

It is interesting to view how the clump members disperse in time in the domain of proper frequencies and elements. Fig. 16 displays projections in the (a, sin(i)) and (g, $g + s$) planes of the orbital evolution of the (6246) clumps clones at $t = 0$ Myr (panels a and b), $t = 50$ Myr (panels c and d) and $t = 100$ Myr (panels e and f). As can be seen in the figure, the clump clones migrate towards smaller and

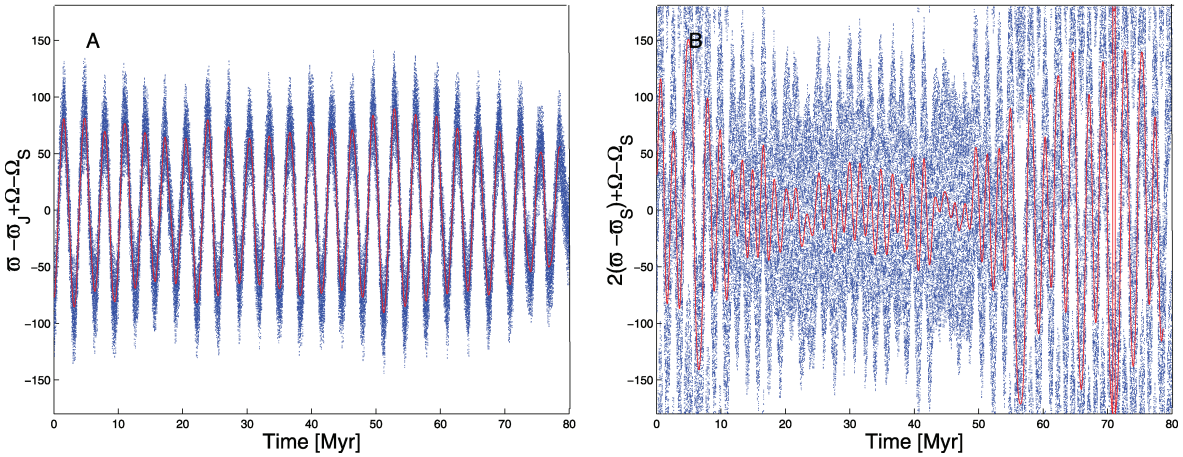

Figure 14. The resonant angles for particles trapped in (a) the $\nu_5 + \nu_{16}$ resonance and (b) the $2\nu_6 - \nu_{16}$ resonance.

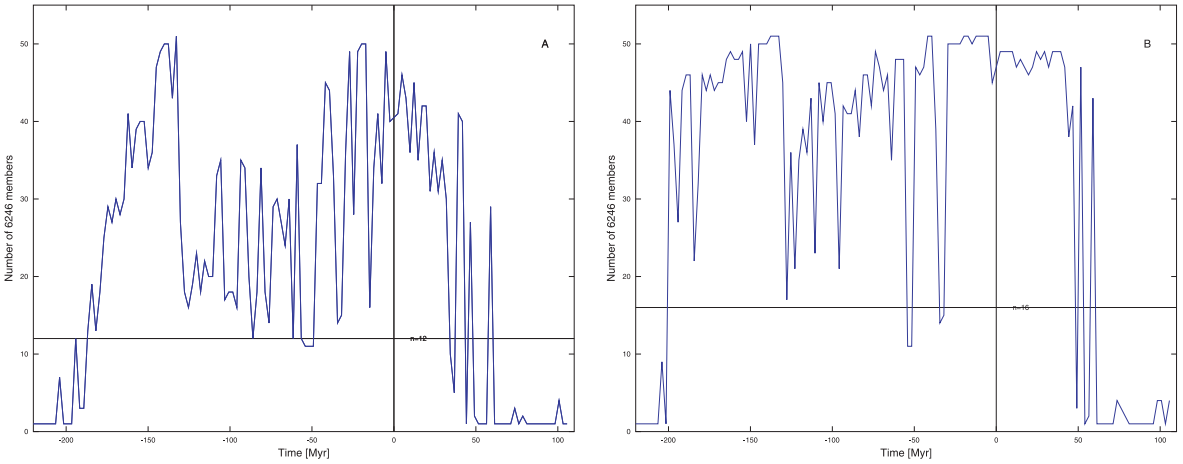

Figure 15. The number of members of the 6246 frequency clumps in the Phocaea family region as a function of time. (a) displays the data for a frequency cut-off of 0.625 arcsec yr^{-1}, while (b) shows the same for a cut-off of 0.745 arcsec yr^{-1}.

higher values of the semi-major axis, depending on their inclination. Several of the test particles are at least temporarily captured in the $\nu_5 + \nu_{16}$ secular resonance (yellow full dots), while fewer experience phases of libration in the $2\nu_6 - \nu_{16}$ resonance (red full dots). Blue circles display the member of the frequency clump, identified in the $(n, g, g + s)$ domain at a cut-off of 0.625 arcsec yr^{-1}. Notice how after 50 Myr the group essentially dispersed and was no longer identifiable as such. Since I am using maximal Yarkovsky drift, this time sets a lower limit on the dynamical stability of the (6246) clump.

I then proceeded with the analysis of the (19536) (1999 JM4) clump. As discussed in Section 6.1, this clump is characterized by its interaction with the $\nu_6 - 2\nu_{16}$ secular resonance. At the beginning of the integration there were 13 particles, the resonant argument of which was in a $\nu_6 - 2\nu_{16}$ librating state. The maximum frequency cut-off for which the clump was still distinguishable from the Phocaea family was 0.625 arcsec yr^{-1}, which was also the nominal cut-off used to determine all frequency groupings in Carruba (2009a).

Fig. 17(a) displays the number of members of the 19563 clump as a function of time, at a cut-off of 0.625 arcsec yr^{-1}. As for the case of the clump around (6246), this clump is detectable until a time of $\simeq$ 30 Myr, and has episodes of observability up to 95 Myr. This seems to suggest that the clump should be statistically significant.

Fig. 17(b) displays a $(g, g + s)$ projection of the clump clones at $t = 27$ Myr, the last time before the clump was no longer identifiable for the first time. Red full dots are asteroids in a librating $\nu_6 - 2\nu_{16}$ resonant state; the other symbols are the same as in Fig. 16. While eight objects were captured in the resonance at this time, the remaining 30 were already evolving far from the resonance separatrix. At $t = 30$ Myr the clump was no longer identifiable, and while there were episodes when the clump was still detectable at later times, after 100 Myr the clump was finally too dispersed to be identifiable. Based on these data, and considering that that the classical family around (19536) was observable for times up to 200 Myr, I believe that the frequency clump around (19536) should be considered statistically significant.

7 CONCLUSIONS

In this work I studied the dynamical evolution of asteroids in the region of the Phocaea dynamical family. This involved the following:

(i) I investigated the long-term stability of asteroids at high e ($e > 0.31$). I found that these objects are unstable on time-scales of at most 270 Myr. Among the mechanisms that can create this high-eccentricity population, the interaction of the Yarkovsky and

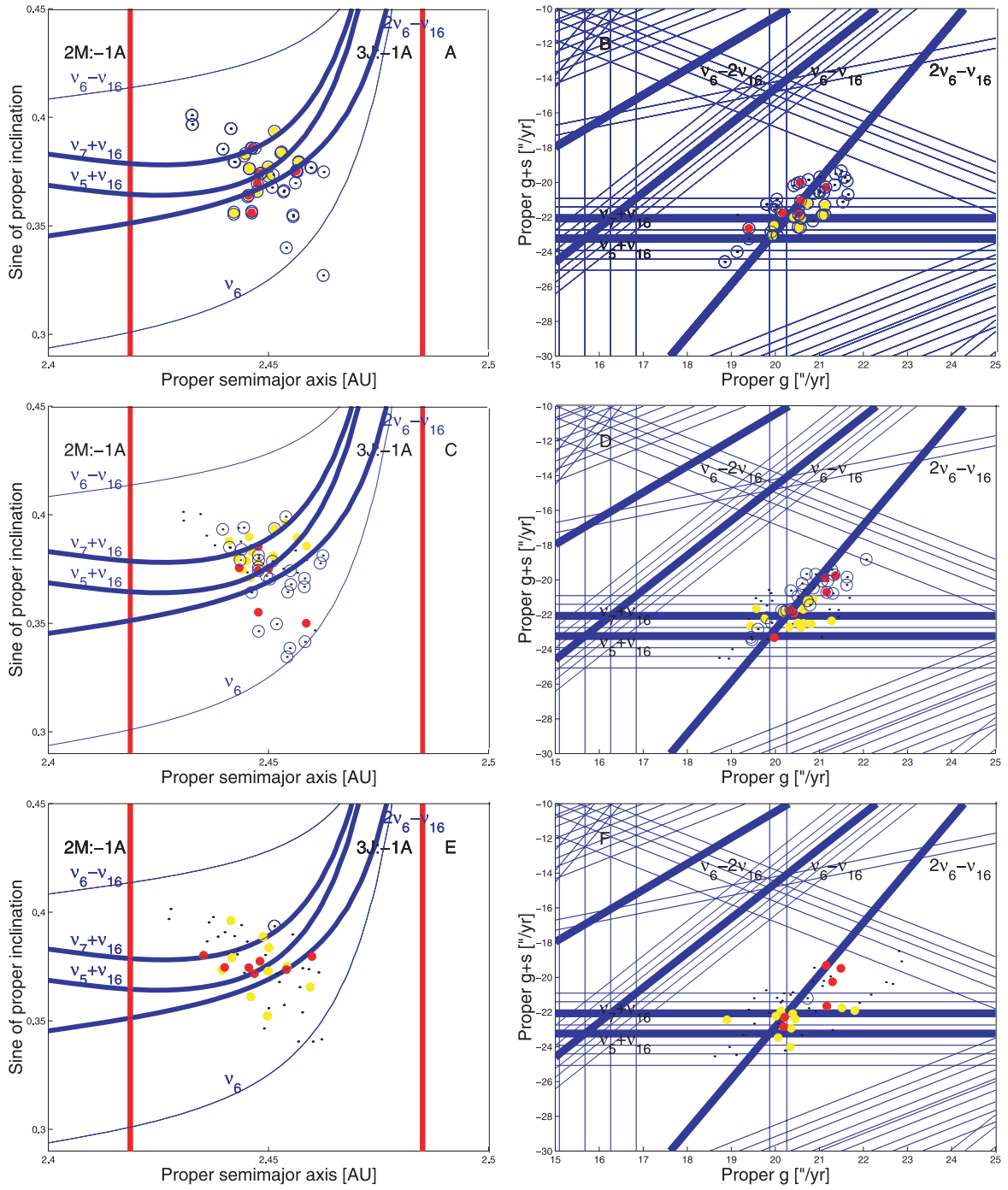

Figure 16. Projections in the $(a, \sin(i))$ and $(g, g+s)$ planes of the orbital evolution of the (6246) clumps clones at $t = 0$ Myr (panels a and b), $t = 50$ Myr (panels c and d) and $t = 100$ Myr (panels e and f).

YORP effects with the J3:–1A, J7:–2A and M2:–1A resonances are the most effective ones. The time needed for current members of the Phocaea family to replenish this population is of the order of 370 Myr. This set a lower limit on the Phocaea family age of $\simeq$640 Myr.

(ii) I studied the problem of asteroids in the proximity of the ν_6 secular resonance separatrix with analytical (Yoshikawa 1987) and numerical tools. Asteroids in a region with $-2.55 < k_6 < 2.55$ arcsec yr^{-1}, where $k_6 = b - \nu_6$ and b is given by equation (7) and roughly corresponds to the g frequency, are forced to reach values of eccentricity larger than 0.31, which is enough to allow them to experience deep close encounters with Mars. The region of $-2.55 < k_6 < 2.55$ arcsec yr^{-1} is associated with the chaotic low-inclination region found in Carruba (2009b) (see Figs 11a and b).

(iii) I investigated the dynamical evolution of the five minor clumps and families identified in Carruba (2009b) in the domain of proper elements and frequencies when the Yarkovsky effect was considered. While the two classical clumps around (17628) and (26142) quickly disperse and seem not to be statistically robust, the family around (19536) is observable for time-scales of 200 Myr for the proper element group, and 50 Myr for the proper frequency

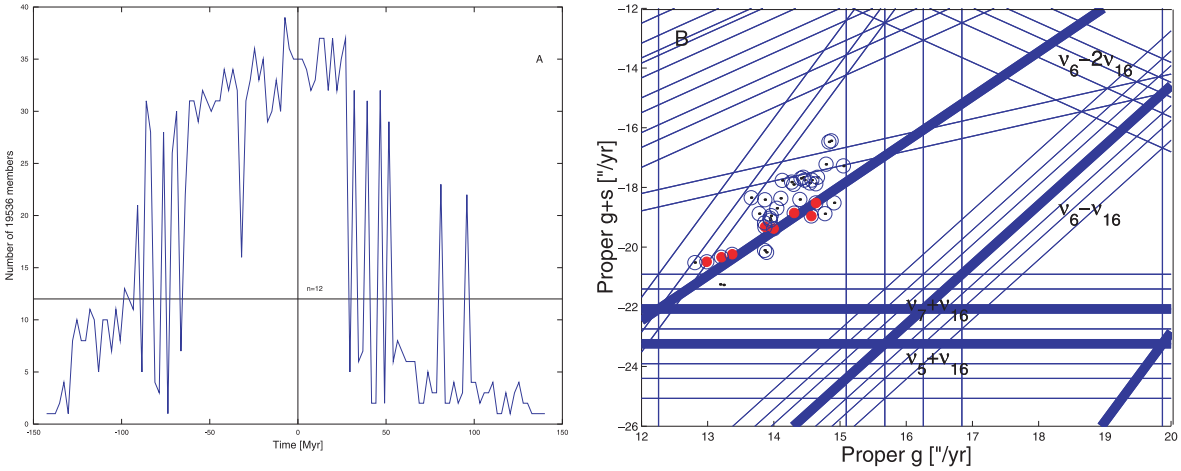

Figure 17. (a) The number of members of the 19536 frequency clump detected at a cut-off of 0.625 arcsec yr^{-1} as a function of time. (b) A $(g, g - s)$ projection of the clump clones at $t = 27$ Myr. The blue circles identify the clump members, the red full dots the asteroids in a librating $\nu_6 - 2\nu_{16}$ resonant state.

clump. I believe that this family should be considered a candidate for a collisional group. Finally, the clump around (6246) Komurotoru, only identifiable in the frequency domain and characterized by its interaction with the $\nu_5 + \nu_{16}$ and $2\nu_6 - \nu_{16}$ secular resonances, is robust on time-scales of 50 Myr. I confirm that this group could be the first clump ever detected in the frequency domain alone that might be associated with a real collisional event.

I believe that this paper provides some answers to and further insights on the main questions raised by Carruba (2009b), i.e. the long-term stability of high-eccentricity objects, the causes of the layer of chaos near the ν_6 resonance separatrix and the statistical significance of the minor groups identified in the Phocaea family region. As often in science, other questions that were raised in these two works are still left unanswered, among them the following: Can I obtain better estimates of the Phocaea family age than those obtained in this and the previous work? How much mass was lost due to the dynamical erosion mechanisms described in this paper and how massive was the original parent body? Also, the fact that the two frequency groups around (19536) and (6246) are statistically significant does not yet prove that these two groups were created by collisions rather than by an aggregation of objects inside secular resonances.

A way to investigate this issue would be to obtain information on the taxonomy of the members of this groups. If they all share a common origin, it would be reasonable to expect that most of the members would have the same spectral type. Unfortunately, such information is not available for these objects. For SDSS-MOC4 data, as discussed in Carruba (2009b), three members of the (19536) group (all compatible with an S-type composition) are reported in the catalogue, while just one member of the (6246) group (yet another S-type compatible object) is currently listed.

In summary, at the moment we cannot rule out either hypothesis on the origin of these groups. Lists of members of the two groups are available to the observing community upon request. In any case, these and other questions on Phocaea asteroid groups remain, in my opinion, interesting subjects for future work.

ACKNOWLEDGMENTS

I am grateful to the reviewer of this article, David A. Minton, for suggestions and comments that helped improve the content of this paper. I thank the São Paulo State Science Foundation (FAPESP), which supported this work via the grant 06/50005-5, and the Brazilian National Research Council (CNPq, grants 302183/2008-6 and 473345/2009-9). I am also grateful to the Mathematics department of FEG-UNESP for the use of their facilities.

REFERENCES

Bretagnon P., 1974, A&A, 30, 141
Brož M., 1999, MSc thesis, Charles Univ., Prague
Carruba V., 2009a, MNRAS, 395, 358
Carruba V., 2009b, MNRAS, 398, 1512
Carruba V., Michtchenko T., 2007, A&A, 475, 1145
Carruba V., Michtchenko T., 2009, A&A, 493, 267
Carruba V., Burns J. A., Nicholson P. D., Gladman B., 2002, Icarus, 158, 434
Carruba V., Burns J. A., Bottke W., Nesvorný D., 2003, Icarus, 162, 308
Carruba V., Nesvorný D., Burns J. A., Cuk M., Tsiganis K., 2004, AJ, 128, 1899
Carruba V., Michtchenko T., Roig F., Ferraz-Mello S., Nesvorný D., 2005, A&A, 441, 819
Carruba V., Roig F., Michtchenko T., Ferraz-Mello S., Nesvorný D., 2007, A&A, 465, 315
Ferraz-Mello S., Klafke J. C., Michtchenko T., Nesvorný D., 1996, Celest. Mech. Dynamical Astron., 64, 93
Gladman B. J. et al., 1997, Sci, 277, 197
Gronchi G. F., Milani A., 1999, A&A, 341, 928
Guillens S. A., Vieira Martins R., Gomes R. S., 2002, AJ, 124, 2322
Knežević Z., Milani A., 2000, Celest. Mech. Dynamical Astron., 78, 17
Knežević Z., Milani A., 2003, A&A, 403, 1165
Levison H. F., Duncan M. J., 2000, AJ, 120, 2117
Milani A., Knežević Z., 1994, Icarus, 107, 219
Morbidelli A., Vokrouhlický D., 2003, Icarus, 163, 120
Murray C. D., Dermott S. F., 1999, Solar System Dynamics. Cambridge Univ. Press, Cambridge
Nesvorný D., Roig F., Gladman B., Lazzaro D., Carruba V., Mothé-Diniz T., 2008, Icarus, 183, 85
Thomas F., Morbidelli A., 1996, Celest. Mech., 64, 209
Yoshikawa M., 1987, Celest. Mech., 40, 233

This paper has been typeset from a TEX/LATEX file prepared by the author.